Chemical Geology 581 (2021) 120405

Contents lists available at ScienceDirect

Chemical Geology

journal homepage: www.elsevier.com/locate/chemgeo

Invited research article

Possible discontinuous evolution of atmospheric xenon suggested by Archean barites

Matthieu G. Almayrac [a,*], Michael W. Broadley [a], David V. Bekaert [a,b], Axel Hofmann [c], Bernard Marty [a]

[a] Université de Lorraine, CNRS, CRPG, F-54000 Nancy, France
[b] Marine Chemistry and Geochemistry Department, Woods Hole Oceanographic Institution, Woods Hole, MA 02543, USA
[c] Department of Geology, University of Johannesburg, Johannesburg, South Africa

ARTICLE INFO

Editor: Don Porcelli

Keywords:
Archean barite
Noble gases
Xenon anomalies
Archean atmosphere

ABSTRACT

The Earth's atmosphere has continually evolved since its formation through interactions with the mantle as well as through loss of volatile species to space. Atmospheric xenon isotopes show a unique and progressive evolution during the Archean that stopped around the Archean-Proterozoic transition. The Xe isotope composition of the early atmosphere has been previously documented through the analysis of fluid inclusions trapped within quartz and barite. Whether this evolution was continuous or not is unclear, requiring additional analyses of ancient samples, which may potentially retain remnants of the ancient atmosphere. Here we present new argon, krypton and xenon isotopic data from a suite of Archean and Proterozoic barites ranging in age from 3.5 to 1.8 Ga, with the goal of providing further insights in to the evolution of atmospheric Xe, whilst also outlining the potential complications that can arise when using barites as a record of past atmospheres. Xenon released by low temperature pyrolysis and crushing of two samples which presumably formed around 2.8 and 2.6 Ga show Xe isotope mass dependent fractionation (MDF) of 11‰.u^{-1} and 3.4‰.u^{-1}, respectively, relative to modern atmosphere. If trapped Xe is contemporaneous with the respective formation age, the significant difference in the degree of fractionation between the two samples provides supporting evidence for a plateau in the MDF-Xe evolution between 3.3 Ga and 2.8 Ga, followed by a rapid evolution at 2.8–2.6 Ga. This sharp decrease in MDF-Xe degree suggests the potential for a discontinuous temporal evolution of atmospheric Xe isotopes, which could have far reaching implications regarding current physical models of the early evolution of the Earth's atmosphere.

1. Introduction

The evolutionary history of the Earth's atmosphere can be elucidated through the analysis of atmospheric remnants residing within the geological record. Due to their chemical inertness, noble gases constitute powerful tracers of the physical processes that have occurred in the atmosphere since its formation. Previous analyses of Archean, Proterozoic and Phanerozoic rocks have shown that some specific samples have kept a record of the ancient atmosphere at different stages of its evolution (Cadogan, 1977; Pujol et al., 2011; Pujol et al., 2013; Stuart et al., 2016; Avice et al., 2017; Avice et al., 2018; Bekaert et al., 2018). Among the noble gases, xenon is the most promising to decipher the early evolution of the atmosphere. Xenon isotopes trapped in fluid inclusions and organic matter residing in Archean-aged rocks have been shown to have isotopic compositions intermediate between the modern atmospheric value and planetary precursors, indicating the atmosphere progressively evolved through time via mass dependent fractionation (MDF; Pujol et al., 2011; Avice et al., 2017). Specifically, Xe isotopic signatures measured in Archean-aged samples show that the ancient atmosphere was enriched in light isotopes relative to its present-day composition, and that the degree of mass fractionation relative to its modern composition decreased with time, finally reaching its current composition at around ~2 Ga (Avice et al., 2018).

Modern atmospheric Xe is fractionated by ~30–40‰ per atomic mass unit (u) relative to its presumed initial composition (U—Xe, Pepin, 1991; Marty et al., 2017). Because isotope fractionation appears to be limited to Xe (Pujol et al., 2011; Avice et al., 2018), a thermal (mass-dependent) process is unlikely to be responsible for Xe escape to space. Xenon does however have a lower first ionization potential than other noble gases (Hébrard and Marty, 2014; Zahnle et al., 2019). Notably

* Corresponding author.
E-mail address: matthieu.almayrac@univ-lorraine.fr (M.G. Almayrac).

https://doi.org/10.1016/j.chemgeo.2021.120405
Received 8 January 2021; Received in revised form 7 May 2021; Accepted 22 June 2021
Available online 25 June 2021

solar UV photons with wavelengths below 100 nm that are able to ionize Xe were potentially more abundant during the Archean and the Hadean eons than today (Ribas et al., 2005). Hébrard and Marty (2014) proposed that the formation of organic haze in the high atmosphere could preferentially trap heavy Xe^+ isotopes, thus preferentially retaining atmospheric Xe heavy isotopes relative to the escaping, lighter ones. However, this model did not detail the mechanism by which Xe^+ escaped to space. A more recent model proposed that escaping hydrogen ions formed by the photo-dissociation of water vapour were able to drag Xe^+ up, with the lighter isotopes escaping to space more easily than the heavier ones (Zahnle et al., 2019). In this model, Xe escaped as an ion lifted up by H^+ along polar magnetic field lines, hence requiring both high-energy EUV (extreme ultra-violet) irradiation from the young Sun and a H-rich atmosphere during the Archean eon relative to modern composition, until the Great Oxidation Event. This Xe-escape mechanism could potentially solve both features of the "xenon paradox" (Ozima and Podosek, 2002): (i) Xe elemental depletion by a factor of ~10 compared to the expected noble gas elemental pattern defined by chondrites (Ozima and Podosek, 2002; Bekaert et al., 2020a), and (ii) isotopic fractionation favouring the heavy Xe isotopes relative to potential cosmochemical precursors.

Determining whether the progressive isotopic evolution of atmospheric Xe was continuous, or not, could provide unique constraints on the evolution of solar activity and Sun-Earth interactions (Ribas et al., 2005; Claire et al., 2012; Zahnle et al., 2019), episodes of extreme mantle degassing (Abbott and Isley, 2002; Marty et al., 2019), and the relationship between atmospheric escape processes and the Great Oxidation Event (Gumsley et al., 2017). To document further the evolution of atmospheric Xe isotopic composition, additional analyses of xenon isotopes trapped in ancient rocks are needed. Barites are promising candidates because of their pervasiveness during the Archean eon and high preservation potential thanks to their low reactivity (Huston and Logan, 2004). Previous works have shown that xenon in barites is in isotopic equilibrium with the atmosphere at the moment of their formation, potentially providing a compositional record of the ancient atmosphere (Meshik et al., 2001; Pujol et al., 2009). This approach requires the samples, in particular the host phases of trapped noble gases, to be accurately dated, which can be challenging as barites are often secondary with respect to the main rock formation (e.g., hydrothermal veins or secondary replacement; Heinrichs and Reimer, 1977).

One promising avenue for providing accurate ages for Archean barites is to use the radioactive decay of ^{130}Ba (~0.1% isotopic abundance) to ^{130}Xe (Meshik et al., 2001; Pujol et al., 2009). Two main decay chains through which ^{130}Xe is produced from Ba are the double β^+ decay ($2\beta^+$) and the double electron capture (2EC) on ^{130}Ba. The primary decay is 2EC with a half-life historically estimated from proton-neutron quasi-particle random phase approximations (*pn*-QRPAs) to be 4.2×10^{21} yr (Hirsch et al., 1994). From the analysis of 200 Ma barites, Meshik et al. (2001) estimated the half-life to be $2.2 \pm 0.5 \times 10^{21}$ yr, consistent with the model-derived value. Subsequently, Pujol et al. (2009) obtained a value of $6.0 \pm 1.1 \times 10^{20}$ yr, one order of magnitude lower than what had been previously proposed, from the analysis of Archean (3.5 Ga) barite from the North Pole formation (Australia). Meshik and Pravdivtseva (2017) questioned this determination by arguing that ^{130}Xe could have been contributed by Xe isotopes produced by cosmic rays at the surface of the Earth. Using the same data set, Meshik and Pravdivtseva (2017) hence estimated the low limit for this half-life to be $>2.4 \times 10^{21}$ yr after correction for cosmogenic effects, more in line with previous estimates (Meshik et al., 2001). These discrepancies highlight the inherent uncertainty associated with the ^{130}Ba—^{130}Xe dating method, and underscore the need for all the potential secondary Xe productions in barites to be thoroughly described and quantified.

Given that barites can be affected by secondary productions of Xe, using barites as an archive of ancient atmospheric Xe requires the careful deconvolution of different potential Xe components. The main production pathways for Xe within barites are from (i) spontaneous fissions of ^{238}U ($T_{1/2} = 4.47$ Gyr) which produces $^{131,132,134,136}Xe$, (ii) interactions between galactic cosmic rays (GCR) and heavy elements such as Ba at the surface of the Earth that significantly produce $^{124,126,128,129,130}Xe$ through spallation reactions, (iii) neutron activation (with neutrons being thermalized from GCR or nuclear reactions within the crust), and finally (iv) other radioactivity reactions such as the decay of ^{130}Ba (Meshik et al., 2001). Using barites as an atmospheric archive therefore requires the successful deconvolution of the five potential Xe components: fractionated Xe from the ancient atmosphere (hereafter Xe_{AA}), fissiogenic Xe (hereafter Xe_f), cosmogenic Xe (hereafter Xe_c), $^{130}Xe^*$ from the radioactive decay of ^{130}Ba, and modern atmospheric Xe (hereafter Xe_{MA}) adsorbed onto grain surfaces or trapped in alteration phases from more recent fluids. In this work, we have undertaken high precision measurements of Ar, Kr and Xe elemental and isotopic compositions in a suite of barites with purported ages ranging from 1.8 to 3.4 Ga, in order to re-evaluate the usefulness of barites as archive for Archean atmospheric Xe.

2. Samples

A series of five barite samples were selected for this study. All samples originate from the Kalahari Craton in South Africa and Zimbabwe. Samples BAVE1 and BAFT11 are from the Barberton greenstone belt (South Africa), sample LPB4 is from the Limpopo Belt (South Africa), and samples Z10/6 and DM4 are from Zimbabwean deposits mined for barites in the past. The samples range in age from ~1.8 Ga (LPB4) to 3.5 Ga (BAVE1). As described below, these ages originate from the surrounding rock units and constitute either maximum or formation ages for the barites and trapped Xe.

Barite samples from the Barberton greenstone belt have a sedimentary-exhalative origin (Reimer, 1980). Sample BAVE1 is from the Theespruit Formation and is associated with felsic volcaniclastic rocks that have been dated by U—Pb on zircon and bulk Sm—Nd methods at 3.53 Ga (Van Kranendonk et al., 2009). The sample consists of an intergrowth of barite and quartz crystals and has a granoblastic texture, which is related to amphibolite-grade metamorphism the rocks experienced at 3.23 Ga. BAFT11 barite sample is derived from the Mapepe Formation of the Fig Tree Group date at ~3.26 Ga (Heinrichs and Reimer, 1977; Drabon et al., 2019). It consists of partially recrystallized barite crystals (mm-cm size) in a sandy matrix of reworked barite crystals.

Z10/6 and DM4 represent coarsely crystalline barite sampled from veins at Argosy and Dodge mines, Zimbabwe, respectively. Barite crystals show some growth banding defined by fluid inclusions, although secondary inclusions trails are also present. The veins are associated with Archean lithologies and have been subjected to deformation and regional metamorphism (Reimer, 1990), regarded to have taken place at ~2.6 Ga (Jelsma and Dirks, 2002). The barite sample Z10/6 was collected from veins that are associated with <2.90 Ga Belingwean to Bulawayan Group greenstone successions (Wilson et al., 1995) and undated, but likely Neoarchaean granitoids, therefore constraining the age of Z10/6 to between 2.60 and 2.90 Ga. In the following we use an approximate age of 2.8 Ga for this sample.

At Dodge mine, sample DM4 barite was taken from a stratiform horizon within Bulawayan greenstones as described by Reimer (1990). The absolute age of the barite is unknown, but on the basis of field relationships it likely formed between 2.60 and ~ 2.70 Ga, the maximum age of the greenstones around the mine (Jelsma and Dirks, 2002). In the following we use an approximate age of 2.6 Ga for this sample.

LPB4 barite, from the Paleoproterozoic red bed succession of the Soutpansberg Group (Reimer, 1995), has a maximum age of 1.85 Ga, as suggested by U—Pb dating of zircons (Geng et al., 2014). Samples contain both detrital barite and *syn*-sedimentary to early diagenetic barite crystals (mm-size) with well developed growth zoning defined by variations in fluid inclusion abundance.

3. Methods

3.1. Bulk chemistry analysis

Aliquots of each sample were analysed for bulk chemistry at the S.A. R.M (Service d'Analyse de Roche et Minéraux), at CRPG, Nancy (France). Abundances of major, minor and trace elements were determined using ICP-OES and ICP-MS (see Carignan et al., 2001 for preparation and analytical methods). Since samples were crushed and dissolved, these results describe only the composition of mineral matrix and not the composition of fluid inclusions. Results are presented in Table S1, Supplementary Material. Among the 55 elements analysed, Ba, K, U, and Th are of particular interest for this study because they can affect noble gas isotope compositions through secondary processes.

3.2. Sample preparation for noble gas mass spectrometry

Barite samples were prepared for noble gas analysis by firstly gently crushing aliquots of the samples into 1–5 mm sized chips. Grains smaller than 1 mm were removed to limit contamination of atmospheric Xe adsorbed onto the grains (high surface/volume ratios). The remaining grains were then examined and handpicked under a binocular microscope to remove samples exhibiting surficial impurities. Before and after picking, the samples were cleaned with acetone in an ultrasonic bath to remove any dust or organic matter from the surface, and dried in an oven at 90 °C for 30 min. Several aliquots weighing 1 to 2 g were prepared for each barite sample (Table 1).

Ancient atmospheric Xe is expected to be found in both the mineral and fluid phases of the barites. Cosmogenic productions of Xe isotopes (from spallation reaction on Ba isotopes), which can over-print the tenuous Archean atmospheric signature, principally occur, and should remain within the crystalline matrix (see Section 5.1.1). To distinguish between the different Xe components, we utilised both crushing and stepwise heating in an attempt to separate noble gases hosted in fluid inclusions and trapped in mineral lattices. Samples were first loaded in stainless steel crushers (see Avice et al., 2017 for more details), before being baked overnight under high vacuum at 200 °C in order to remove any adsorbed atmospheric noble gases. The samples were then crushed to release the noble gases held within fluid inclusions. Extracted noble gases were circulated through an in-line getter filled with Ti-sponge and silver wool at 600 °C to remove reactive components and sulfur compounds such as SO_2, respectively. Pujol et al. (2009) demonstrated the efficiency of silver wool to purify the enormous amount of SO_2 and O liberated during pyrolysis of barites ($BaSO_4$). The in-line getter was reactivated every few extractions and between each new sample. The silver wool was changed once after half the barites were analysed. For each analysis, the purification of the gas lasted 30 min. Krypton and xenon were then separated from argon using a quartz cold finger held at liquid N_2 temperature for 20 min. Typically, 5% of the Kr and < 1% of the Xe was not trapped in the quartz cold finger and therefore was lost in the Ar fraction, this loss does not produce any significant isotopic fractionation (this was verified by analysing air standards following the same protocol as the sample purification). The remaining Ar was sequentially purified with two series of additional Ti-sponge getters (two at 550 °C and the other two at 60 °C), for 10 min each, before being expanded to the Thermo Fisher Helix MC PLUS mass spectrometer for analysis. Argon was analysed using peak jumping mode, with ^{40}Ar measured on the axial faraday collector and $^{36,38}Ar$ measured on the axial compact dynode electron multiplier. Krypton and xenon were then subsequently released from the quartz finger at room temperature and purified the same way as Ar prior to analysis. Krypton and xenon were admitted to the mass spectrometer simultaneously, although only Xe isotopes were measured during crushing extractions. Xenon isotopes were analysed using peak jumping mode over 20 repeat analytical cycles on the axial compact dynode electron multiplier.

Crushing residues typically weighing ~500 mg (diameter > 750 μm) were recovered, wrapped in tin (Sn) foil and loaded in a stainless steel induction furnace (Zimmermann et al., 2018), which was then baked at 160 °C for 24 h. For this extraction, we used stepwise heating at three different temperature steps of 15 min each: ~800 °C, ~1300 °C and ~1800 °C (Table 2). The released gas was purified and analysed following the same procedure as outlined for crushing, although this time Kr was also analysed just after Xe following the same procedure.

Over the sequence of analyses, the mass spectrometer sensitivity and instrumental mass discrimination were controlled by measuring known standards of gas with known abundances and atmospheric isotopic compositions. Blanks were all essentially atmospheric and were subtracted from the sample analysis. Average blank values, reproducibility and mass discrimination of the mass spectrometer are presented Table S2, Supplementary Material. Typical blanks contributions during crushing extraction for Ar and Xe were < 5% and < 20%, respectively. For step-heating blanks, an empty tin foil was dropped in the furnace crucible and a full 800 °C–1300 °C-1800 °C run was performed. At the 1800 °C temperature step the blank contribution for Kr and Xe was ~50% for both. Due to the high Ar blanks at 1300 °C and 1800 °C steps (higher than the Ar signal of the sample), we do not report the Ar data for the samples at these temperatures. This high blank contribution results from the crucible degassing excessive amount of Ar at high temperature because it was manufactured under an Ar atmosphere (Zimmermann et al., 2018). Ar diffusion from the crucible at 800 °C is small, but becomes more important at >1300 °C steps, hence why we do not report Ar data for the 1300 °C and 1800 °C temperature steps.

Following the approach of Avice et al. (2017), the results for a given sample correspond to the average of all the corresponding aliquots (same experimental and analytical procedure for each aliquots). Errors are calculated using standard error (standard deviation divided by $\sqrt{n-1}$ where n = number of aliquots analysed for a given sample, 1σ; the error propagation method is detailed in Supplementary Material).

4. Results

The abundances and isotopic compositions of noble gases released by crushing and step heating are given in Tables 1,2 and in supplementary tables.

4.1. Crushing results

Argon extracted by crushing of the five barite samples present abundances ranging from 2.84×10^{-12} mol.g^{-1} to 7.00×10^{-9} mol.g^{-1}. Samples DM4 and Z10/6 have maximum $^{40}Ar/^{36}Ar$ ratios up to 1795 ± 8 and 7349 ± 126, respectively, an order of magnitude higher than the modern atmospheric value of 298.6 ± 0.3 (Lee et al., 2006). Samples BAVE1, BAFT11 and LPB4 have $^{40}Ar/^{36}Ar$ ratios of 299.2 ± 0.4, 315.3 ± 0.5 and 345.9 ± 0.5 respectively, closer to the modern atmospheric value (see Ar results Table S3, Supplementary Material).

The abundances of ^{132}Xe extracted by crushing range from 2.04×10^{-17} to 4.04×10^{-14} mol.g^{-1} (Table 1 and Table S4, Supplementary Material), comparable to abundances previously measured in Archean barites (Pujol et al., 2009). Sample LPB4 shows the highest Xe content of 4.04×10^{-14} mol.g^{-1}, which may be the result of higher levels of air contamination considering that the $^{40}Ar/^{36}Ar$ ratio (346) is close to air. Only Z10/6 and DM4 samples have Xe isotopic compositions significantly different from the present atmospheric composition (Fig. 1 and Fig. 2a). DM4-crushing displays excesses for the light isotopes $^{124,126,128,129}Xe$ up to 30‰ (using delta notation, $\delta^{i}Xe = [(^{i}Xe/^{130}Xe)_{sample}/(^{i}Xe/^{130}Xe)_{air} - 1] * 1000$, where *air* refers to the modern atmospheric composition, Basford et al., 1973), and an atmospheric composition for heavy isotopes (Fig. 1). In contrast, Z10/6-crushing shows excesses for the heavy isotopes $^{131,132,134,136}Xe$ ranging from 10‰ to 100‰, suggesting addition of fissiogenic Xe (Porcelli and Ballentine, 2002, Fig. 2a). It also displays possible excesses in the light

Table 1
Xenon abundances and corrected isotopic ratios obtained in the five barites by crushing. Several aliquots were made for sample Z10/6, DM4. All aliquots were crushed several times to ensure all gas was released. If not specified, the second crush did not release gas above blank. Isotopic ratios are normalised to isotope ^{130}Xe, see Table S4 for normalization to ^{132}Xe.

Sample	#	Mass (g)	^{132}Xe (10^{-17} mol.g^{-1})	±	$^{124}Xe/^{130}Xe$	±	$^{126}Xe/^{130}Xe$	±	$^{128}Xe/^{130}Xe$	±	$^{129}Xe/^{130}Xe$	±	$^{131}Xe/^{130}Xe$	±	$^{132}Xe/^{130}Xe$	±	$^{134}Xe/^{130}Xe$	±	$^{136}Xe/^{130}Xe$	±
Z10/6	1	1.919	75.68	1.32	0.02400	0.00095	0.02079	0.00096	0.47424	0.01267	6.51423	0.15779	5.24632	0.12730	6.75400	0.16339	2.74699	0.06731	2.40574	0.05936
	2 first crush	1.639	194.50	4.02	0.02345	0.00088	0.02267	0.00083	0.47092	0.01397	6.48535	0.18296	5.24695	0.15013	6.73519	0.19122	2.76423	0.07999	2.42147	0.07053
	2 s crush	–	339.00	5.27	0.02404	0.00068	0.02205	0.00077	0.47249	0.01044	6.50102	0.13738	5.28248	0.11014	6.73179	0.14148	2.71788	0.05696	2.38690	0.05173
			533.50	6.62																
DM4	1	0.966	166.75	3.20	0.02432	0.00105	0.02214	0.00117	0.46505	0.01264	6.51344	0.16783	5.20964	0.13446	6.57442	0.16934	2.55486	0.06784	2.17353	0.05829
	2	1.985	30.70	0.17	0.02381	0.00031	0.02217	0.00028	0.47445	0.00397	6.52545	0.05163	5.22933	0.04110	6.62750	0.05193	2.55546	0.02047	2.16490	0.01711
	3 first crush	1.527	101.05	2.22	0.02364	0.00124	0.02247	0.00122	0.47359	0.01596	6.52230	0.19496	5.24709	0.15552	6.63126	0.19667	2.57255	0.07618	2.19631	0.06849
	3 s crush	–	153.21	2.90	0.02388	0.00074	0.02160	0.00099	0.47773	0.01291	6.51065	0.16421	5.21807	0.13174	6.62121	0.16824	2.55637	0.06594	2.17427	0.05559
			254.26	3.65																
LPB4	1 first crush	1.076	3980.41	134.90	0.02289	0.00122	0.02250	0.00131	0.45989	0.02240	6.47736	0.30797	5.20978	0.24862	6.61769	0.31398	2.54873	0.12167	2.14794	0.10258
	1 s crush	–	61.24	1.58	0.02113	0.00125	0.02112	0.00116	0.45337	0.01812	6.51887	0.22978	5.23848	0.18646	6.62825	0.23264	2.53771	0.09180	2.17931	0.08157
			4041.65	134.91																
BAFT11	1	2.011	128.72	1.90	0.02142	0.00082	0.02122	0.00068	0.45434	0.01071	6.41350	0.13006	5.17858	0.10563	6.49371	0.12981	2.51127	0.05274	2.13681	0.04409
BAVE1	1	1.396	2.04	0.06	0.02253	0.00109	0.02440	0.00111	0.47135	0.01827	6.47435	0.23869	5.23958	0.19434	6.59297	0.24601	2.53556	0.09447	2.14732	0.08016
Atmosphere		Basford et al. (1973)			0.02337	0.00008	0.02180	0.00011	0.47150	0.00070	6.49600	0.00900	5.21300	0.00800	6.60700	0.00500	2.56300	0.00400	2.17600	0.00300

Table 2
Xenon abundances and corrected isotopic ratios obtained in the five barites by heating at 800 °C, 1300 °C and 1800 °C. Isotopic ratios are normalised to ^{132}Xe, see Table S7 for normalization to ^{130}Xe. Sample DM4 aliquot 3 at 1800 °C is lower than blank. The 1300 °C and 1800 °C steps of aliquot one for sample BAFT11 was omitted from the average since it is different from the two other aliquots at 3σ.

Sample	#	Mass (g)	Heating step (°C)	^{132}Xe (10^{-17} mol. g-1)	±	$^{124}Xe/^{132}Xe$	±	$^{126}Xe/^{132}Xe$	±	$^{128}Xe/^{132}Xe$	±	$^{129}Xe/^{132}Xe$	±	$^{130}Xe/^{132}Xe$	±	$^{131}Xe/^{132}Xe$	±	$^{134}Xe/^{132}Xe$	±	$^{136}Xe/^{132}Xe$	±
Z10/6	1	0.425	800 °C	5.33	0.05	0.00367		0.00085	0.00342	0.00072	0.07444	0.00524	0.98358	0.03081	0.15023	0.00901	0.79774	0.02361	0.40659	0.01656	0.35194	0.01219
			1300 °C	2.02	0.04	0.00524		0.00060	0.00775	0.00106	0.07979	0.00389	0.98012	0.01902	0.15756	0.00693	0.94041	0.01950	0.38134	0.00986	0.32795	0.00716
			1800 °C	4.21	0.03	0.00454		0.00065	0.00663	0.00099	0.07757	0.00348	0.97386	0.01903	0.16309	0.00521	0.89135	0.01873	0.37847	0.01102	0.33631	0.00876
	2	0.603	800 °C	10.04	0.08	0.00364		0.00045	0.00349	0.00049	0.07069	0.00326	0.97131	0.01954	0.14923	0.00602	0.77978	0.01900	0.41081	0.00889	0.36178	0.00930
			1300 °C	13.52	0.11	0.00584		0.00055	0.00762	0.00071	0.07953	0.00269	0.97862	0.01655	0.15873	0.00514	0.94975	0.02162	0.39829	0.01025	0.34270	0.00905
			1800 °C	10.20	0.08	0.00451		0.00067	0.00431	0.00061	0.07227	0.00299	0.98690	0.01914	0.15272	0.00433	0.83078	0.01646	0.38362	0.00906	0.33338	0.00741
	3	0.281	800 °C	10.71	0.10	0.00385		0.00067	0.00336	0.00061	0.07354	0.00442	0.98341	0.03340	0.14972	0.00870	0.79360	0.01913	0.40476	0.01197	0.34454	0.01148
			1300 °C	10.92	0.12	0.00610		0.00077	0.00874	0.00153	0.08249	0.00532	0.99671	0.01873	0.16098	0.00616	0.98924	0.03855	0.39304	0.01156	0.34174	0.00849
			1800 °C	9.64	0.09	0.00426		0.00050	0.00383	0.00064	0.07522	0.00344	0.98806	0.02345	0.15655	0.00435	0.79366	0.02033	0.38769	0.01303	0.33325	0.01094
	4	0.382	800 °C	5.66	0.08	0.00354		0.00102	0.00353	0.00061	0.07425	0.00456	0.98588	0.03629	0.15426	0.00747	0.79588	0.02857	0.39849	0.01441	0.34582	0.01617
			1300 °C	12.74	0.11	0.00636		0.00072	0.00783	0.00110	0.07808	0.00402	0.99728	0.02384	0.15983	0.00487	0.98472	0.02649	0.39186	0.00794	0.32911	0.01114
			1800 °C	5.69	0.06	0.00451		0.00061	0.00438	0.00048	0.09280	0.00434	0.98390	0.02246	0.15638	0.00629	0.81548	0.01960	0.38466	0.00967	0.32774	0.00895
DM4	1	0.336	800 °C	4.91	0.09	0.00377		0.00068	0.00320	0.00046	0.09052	0.00622	0.97674	0.02901	0.15311	0.00861	0.78622	0.02882	0.38125	0.01799	0.33325	0.01392
			1300 °C	3.67	0.06	0.00461		0.00115	0.00420	0.00076	0.07187	0.00755	0.96813	0.04729	0.15285	0.01252	0.81724	0.03360	0.38638	0.01632	0.32237	0.01444
			1800 °C	4.48	0.06	0.00357		0.00065	0.00311	0.00052	0.07651	0.00424	0.99950	0.02988	0.15970	0.00718	0.79852	0.02700	0.39059	0.01368	0.34371	0.01262
	2	0.809	800 °C	13.50	0.08	0.00362		0.00025	0.00323	0.00044	0.07121	0.00263	0.98756	0.01227	0.15215	0.00326	0.78740	0.01388	0.38786	0.00789	0.32760	0.00708
			1300 °C	32.34	0.19	0.00369		0.00024	0.00348	0.00031	0.07179	0.00276	0.98765	0.01426	0.15276	0.00286	0.78986	0.01072	0.38424	0.00500	0.32433	0.00475
			1800 °C	9.06	0.06	0.00379		0.00048	0.00370	0.00045	0.07202	0.00302	0.99022	0.01461	0.15166	0.00448	0.79508	0.01276	0.38636	0.00635	0.32538	0.00631
	3	0.505	800 °C	6.69	0.07	0.00358		0.00066	0.00319	0.00080	0.07552	0.00528	0.98876	0.02999	0.15368	0.00957	0.78709	0.02437	0.38749	0.01438	0.32708	0.01390
			1300 °C	3.05	0.04	0.00387		0.00092	0.00451	0.00061	0.07174	0.00562	1.00024	0.03629	0.15870	0.00951	0.81083	0.02198	0.38046	0.02018	0.32508	0.01559
			1800 °C	–	–	–		–	–	–	–	–	–	–	–	–	–	–	–	–	–	–
LPB4	1	0.506	800 °C	4.56	0.07	0.00331		0.00064	0.00316	0.00045	0.07264	0.00663	0.98997	0.03700	0.15023	0.00903	0.78663	0.02620	0.38773	0.01990	0.32883	0.01517
			1300 °C	3.65	0.05	0.00473		0.00121	0.00546	0.00090	0.07188	0.00558	0.96692	0.03789	0.15148	0.00813	1.35557	0.08185	0.39954	0.01645	0.34666	0.01359
			1800 °C	2.28	0.03	0.00510		0.00090	0.00633	0.00122	0.07776	0.00435	0.97821	0.02810	0.15560	0.00652	1.56903	0.06570	0.39274	0.01262	0.35202	0.01193
BAFT11	1	0.389	800 °C	5.52	0.07	0.00373		0.00081	0.00357	0.00096	0.06986	0.00613	1.00067	0.03702	0.15249	0.00649	0.80393	0.02639	0.38912	0.01507	0.33241	0.01537
			1300 °C	4.31	0.08	0.00411		0.00078	0.00603	0.00127	0.06507	0.00445	0.82818	0.04012	0.13349	0.01075	2.26399	0.30480	0.54647	0.03904	0.53212	0.04323
			1800 °C	4.51	0.07	0.00594		0.00090	0.01078	0.00134	0.07403	0.00445	0.86501	0.02728	0.14639	0.00806	5.04380	0.66279	0.51198	0.02113	0.51034	0.02348
	2	1.039	800 °C	3.94	0.04	0.00349		0.00053	0.00308	0.00044	0.06802	0.00368	0.96813	0.02386	0.14681	0.00568	0.79098	0.02324	0.40813	0.01310	0.35585	0.00956
			1300 °C	7.43	0.06	0.00399		0.00059	0.00604	0.00075	0.04574	0.00411	0.54251	0.05848	0.09062	0.00765	2.71467	0.29101	0.84726	0.07323	0.94723	0.09289
			1800 °C	2.10	0.02	0.00736		0.00111	0.01218	0.00150	0.05828	0.00324	0.55996	0.02958	0.10508	0.00641	6.17832	0.68199	0.80802	0.04000	0.89996	0.06586
	3	0.510	800 °C	4.77	0.09	0.00392		0.00065	0.00345	0.00080	0.07065	0.00534	0.97637	0.03263	0.15092	0.00623	0.79542	0.02739	0.39458	0.01440	0.33880	0.02045
			1300 °C	4.51	0.05	0.00490		0.00089	0.00693	0.00112	0.05702	0.00474	0.66684	0.05260	0.10952	0.00778	2.99626	0.43321	0.72579	0.06335	0.78025	0.08838
			1800 °C	2.19	0.02	0.00725		0.00110	0.01022	0.00137	0.06854	0.00444	0.68524	0.03282	0.11993	0.00616	5.34693	0.65702	0.69441	0.03317	0.74902	0.04253
BAVE1	1	0.420	800 °C	6.65	0.08	0.00351		0.00105	0.00325	0.00087	0.07327	0.00282	0.99106	0.03198	0.14925	0.00736	0.78644	0.03258	0.37720	0.01840	0.33013	0.01673
			1300 °C	3.59	0.03	0.00439		0.00097	0.00548	0.00131	0.07458	0.00442	0.97116	0.02038	0.15216	0.00752	0.88660	0.02658	0.40739	0.01380	0.35320	0.01046
			1800 °C	10.01	0.07	0.00417		0.00062	0.00449	0.00055	0.07145	0.00278	0.97417	0.01514	0.14754	0.00391	0.85140	0.01559	0.40074	0.01404	0.35285	0.00834
	2	0.446	800 °C	4.62	0.07	0.00332		0.00092	0.00323	0.00102	0.07022	0.00454	0.98222	0.03868	0.15294	0.00860	0.77736	0.03108	0.38488	0.01600	0.32147	0.01564
			1300 °C	4.04	0.06	0.00509		0.00101	0.00605	0.00114	0.07494	0.00570	0.96844	0.03679	0.14811	0.00822	0.93505	0.03099	0.40071	0.01618	0.34881	0.01725
			1800 °C	10.99	0.10	0.00402		0.00048	0.00354	0.00043	0.07276	0.00325	0.98075	0.02008	0.14929	0.00396	0.79157	0.01898	0.39581	0.01047	0.34005	0.00766
			Atmosphere	Basford et al. (1973)		0.00353		0.00001	0.0033	0.00002	0.07136	0.0009	0.98320	0.00120	0.15136	0.00012	0.78900	0.00110	0.38790	0.00060	0.32940	0.00040

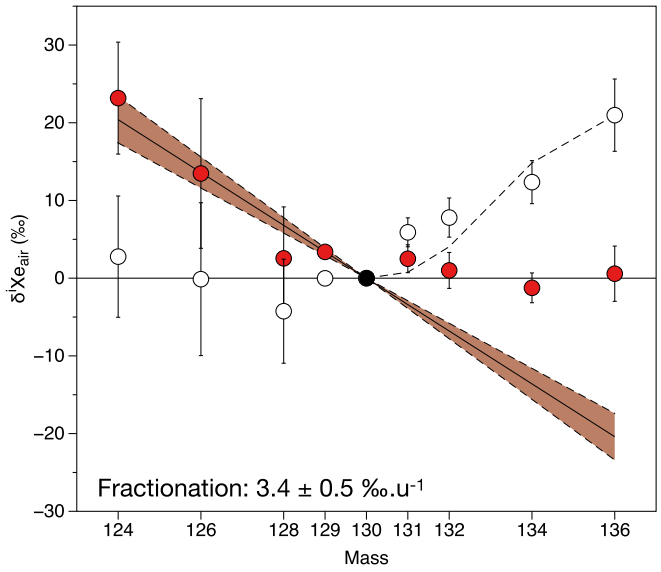

Fig. 1. Xe isotopic composition of the DM4 crushing step (full circles; error bars are 1σ, standard error) in $\delta^{i}Xe$ values (defined as $\delta^{i}Xe = (({}^{i}Xe/{}^{130}Xe)_{sample}/({}^{i}Xe/{}^{130}Xe)_{air} - 1)*1000$, *air* subscript referring to the modern atmospheric composition, Basford et al., 1973). The error bar on isotope ^{129}Xe is smaller than the symbol size. Excesses of $^{124,126,128,129}Xe$ isotopes are consistent with a mass dependent fractionation (MDF) of 3.4 ± 0.5‰.u^{-1} (red shaded area represents 1σ standard error). When corrected for MDF (open symbols), the heavy isotopes spectrum is consistent with contribution of fissiogenic Xe from U (dashed line). (For interpretation of the references to colour in this figure legend, the reader is referred to the web version of this article.)

isotopes, but associated uncertainties are too large, especially for ^{126}Xe, to reach a firm conclusion. Crushing of LPB4, BAFT11 and BAVE1 samples released xenon with isotopic compositions similar to that of the modern atmosphere (Table 1 and Fig. S5,S6,S7, Supplementary Material).

4.2. Step heating results

Argon released at 800 °C (the only step giving Ar signals above blank level) shows ^{40}Ar abundances ranging from 0.65 to 4.42 × 10^{-10} mol.g^{-1}, and $^{40}Ar/^{36}Ar$ up to 13,200 ± 1700 for BAFT11 barite (Table S5, Supplementary Material). Total abundances of ^{84}Kr released during step heating (800 °C, 1300 °C and 1800 °C) range from 1.42 mol.g^{-1} to 7.77 × 10^{-16} mol.g^{-1}. Krypton isotopic ratios measured in the first 6 samples by step heating were similar (within 1σ) to the modern atmospheric composition (Basford et al., 1973), regardless of the temperature step (Table S6, Supplementary Material). Therefore, for the remaining 7 samples, krypton was not analysed.

At the 800 °C extraction step, ^{132}Xe concentrations range from 0.39 mol.g^{-1} to 1.35 × 10^{-16} mol.g^{-1} (Table 2 and Table S7, Supplementary Material). At this step, sample Z10/6 is the only one to exhibit an isotopic signature distinct from that of the atmosphere, with $^{124\text{-}128}Xe/^{130}Xe$ and $^{134,136}Xe/^{130}Xe$ both in excess of atmospheric values (Fig. 2b). Sample DM4, contrary to the crushing extraction, does not show any significant isotopic deviation from the modern atmospheric composition (Fig. S4, Supplementary Material).

At higher temperature, typical ^{132}Xe abundances range from 2.05 mol.g^{-1} to 4.14 × 10^{-16} mol.g^{-1} (total abundance released from the two high temperature steps, Table 2). Xenon fractions released at 1300 °C and 1800 °C are isotopically similar for all samples. To aid simplicity we will therefore use the 1300 °C step in the following section, when discussing the high temperature release. All five samples (Fig. 3, using ^{132}Xe for isotope normalization at high temperature steps) show significant excesses in $^{124,126,128}Xe/^{132}Xe$, with the $^{124,126,128}Xe/^{132}Xe$ ratios being comparable to those expected for cosmogenic production. The samples also exhibit strong monoisotopic excesses of ^{131}Xe, with $\delta^{131}Xe$ values ranging from 20‰ to ~2800‰, for DM4 and BAFT11, respectively. In addition, LPB4, BAFT11 and BAVE1 show excesses in $^{134\text{-}136}Xe$ that are in agreement with the ^{238}U fissiogenic pattern (Fig. 3).

5. Discussion

Crushing and step-heating of the barites revealed a wide spread of xenon isotopic anomalies that result from the simultaneous release of various components. Isotopic spectra are required to be thoroughly deconvoluted and interpreted in order to isolate possible primary signatures inherited from the Archean atmosphere.

5.1. Archean atmosphere trapped in barite fluid inclusions

5.1.1. Decoupling of the fluid inclusions and matrix composition: Components, host phases and diffusion of Xe

Archean barites are expected to possess a variety of noble gas components. This can include components of primary origin, such as the Archean atmosphere or secondary components, resulting from nuclear reactions (U fission, spallation on Ba, ^{130}Ba neutron activation and radioactivity). These components can be hosted in either the fluid inclusions, the matrix, or both. In order to separate the different components held within the fluid inclusions and the matrix, different extraction methods can be employed, with crushing preferentially releasing gas from the fluid inclusions whilst step-heating will release all the remaining gas held within the matrix and un-cracked fluid inclusions. However, it should be noted that the possibility for Xe, and other noble gases to diffuse from one phase to the other could complicate the identification of components, especially the primary ancient atmosphere which is likely to be the most tenuous (~10‰ variations) and subject to overprinting by secondary component (~100–1000‰ variations).

Crushing of Z10/6 barite revealed an unambiguous secondary fissiogenic component Xe_f for isotopes $^{131\text{–}132\text{-}124\text{-}136}Xe$ (Fig. 2a), resulting from the spontaneous fission of ^{238}U. However, bulk chemistry analysis of the matrix revealed that Z10/6 did not contain detectable amount of uranium (Table S1, <0.07 ppm). This is in agreement with the observation that no Xe_f was found from high temperature (1300 °C an 1800 °C) pyrolysis extraction on this barite (Fig. 2c,d). The detection of Xe_f within the fluid inclusion and not the matrix of Z10/6 indicates that either (i) the fluid component already contained excess Xe_f, as it has been shown to be the case for ^{40}Ar (Avice et al., 2017), a likely possibility due to interaction between the fluids and the crust, or (ii) the fluids carried a source of U that was not incorporated into the barite matrix. The absence of Xe_f in the matrix furthermore suggest that Xe from the fluid inclusions has remained isolated since their formation, with limited diffusion of noble gases either in or out.

Conversely, samples BAVE1, LPB4 and BAFT11 have detectable amount of U (0.11 ppm, 0.12 ppm and 1.27 ppm, respectively, Table S1) yet do not present Xe_f during crushing or heating at low temperature (800 °C, Fig. S5–6-7). They do however show large Xe_f excess when heated to higher temperature (1300 °C, Figs. 3 and 1800 °C, Fig. S5–6-7). This indicates that these barites only have U in their matrix, and that the Xe_f component remained in the matrix and did not diffuse in the fluid inclusions.

Taken together, these observations are consistent with little or no diffusion of Xe between fluid inclusions and matrix. Additionally, this confirms that extraction by crushing only liberates gas from fluid inclusions, as does pyrolysis at 800 °C, and that high temperature extraction (1300 °C and 1800 °C) releases gas from the matrix (and any remaining fluid inclusions by extension).

5.1.2. DM4 barite: Ancient atmosphere revealed by crushing

Xenon released during crushing of sample DM4 shows excesses in the

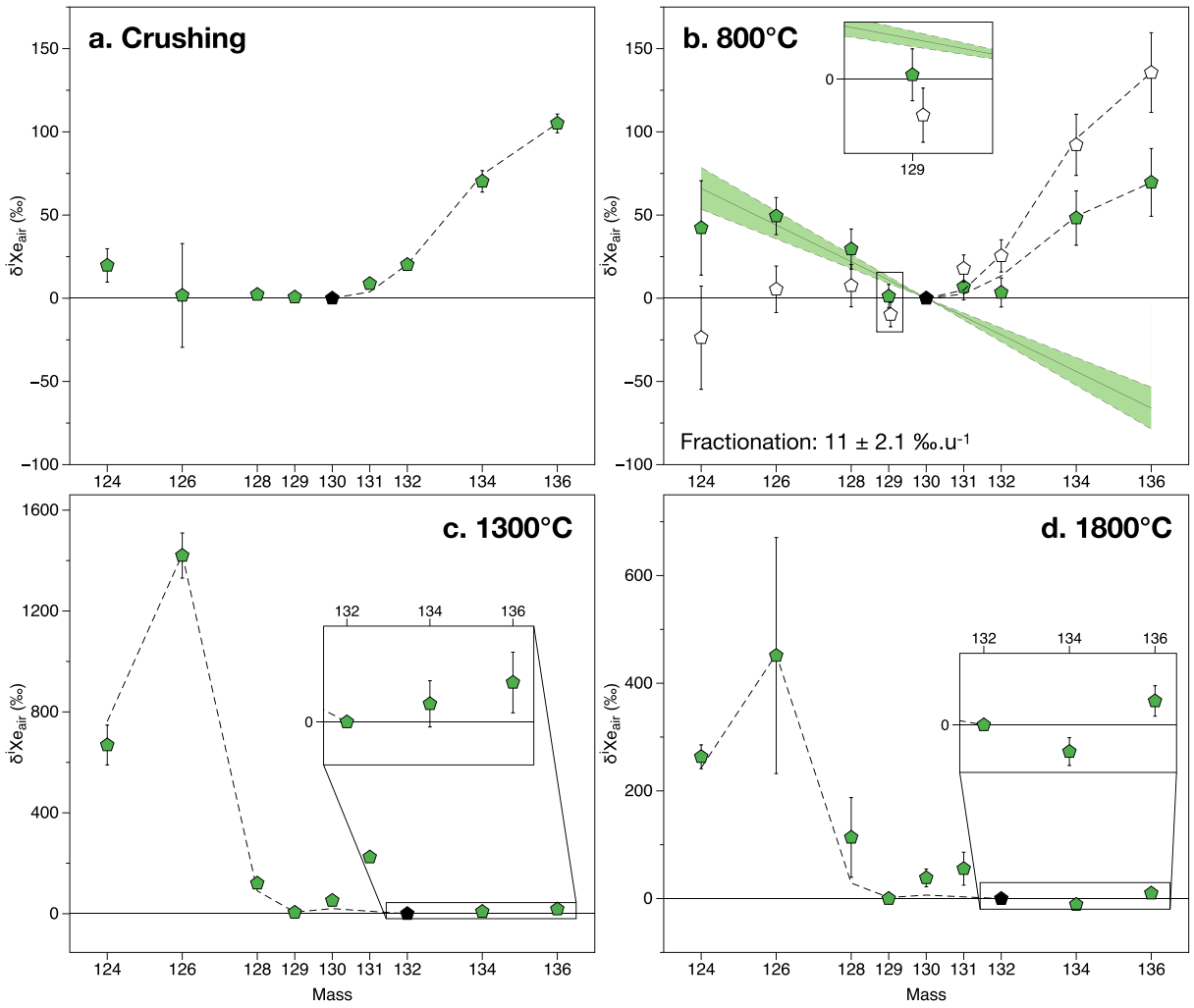

Fig. 2. Isotopic spectra of Xe released by crushing and step-heating of Z10/6 barite. a. Crushing. Excesses of $^{131-136}$Xe are compared with the expected fission spectra of ^{238}U anchored on ^{136}Xe (dashed line). b. 800 °C. Full symbols represent the measured composition. Green shaded area is the MDF fit of 11 ± 2.1‰.u^{-1} (1σ) using light isotopes $^{124-130}$Xe. Open symbols are the measured data corrected for MDF. After correction, the ^{238}U fission spectrum fits the $^{131-136}$Xe excesses (dashed line) as in Fig. 1. Note a depletion of ^{129}Xe relative to the MDF line, as expected for Archean atmospheric Xe (Avice et al., 2017; Marty et al., 2019). c. 1300 °C. Strong evidence for cosmogenic contribution for light isotopes by spallation reaction, monoisotopic excess of ^{131}Xe and negligible excess in δ^{136}Xe = 18 ± 14‰. The dashed line is the fit of the expected production pattern of Xe isotopes from interaction between high-energy particles (300 MeV protons, Kaiser, 1977) and Ba isotopes, anchored on ^{126}Xe. d. 1800 °C. Similar pattern as 1300 °C release, with smaller excesses due do higher atmospheric contamination. Note the difference in normalizing isotopes, ^{130}Xe for crushing and 800 °C steps, and ^{132}Xe for 1300 °C and 1800 °C steps. (For interpretation of the references to colour in this figure legend, the reader is referred to the web version of this article.)

light Xe isotopes ^{124,126,128,129}Xe relative to the modern atmospheric composition (Fig. 1). These excesses decrease systematically from ^{124}Xe to ^{129}Xe, which is consistent with a mass-dependent fractionation (MDF) of 3.4 ± 0.5‰.u^{-1} (1σ, error-weighted linear regression using ^{124,126,128,129,130}Xe with IsoplotR© software, Vermeesch, 2018). Assuming that the noble gases within the fluid inclusions were in isotopic equilibrium with the atmosphere during rock formation, then this MDF signature should be representative of the atmosphere at the time of Xe trapping (Pujol et al., 2011; Pujol et al., 2013; Avice et al., 2017; Avice et al., 2018). When corrected for MDF, the heavy Xe isotopes ($^{131-136}$Xe) are consistent with secondary contribution of fissiogenic $^{131-136}$Xe from ^{238}U (Fig. 1). We therefore suggest that DM4 fluid inclusions possess both a MDF signature and fissiogenic Xe excesses. Although the possibility for the light isotope excesses to results from cosmogenic reactions with Ba cannot be entirely excluded, we consider it unlikely because (i) crushing is unlikely to liberate Xe isotopes produced in the crystal matrix (although in some cases release of cosmogenic He by crushing has been observed, Yokochi et al., 2005; Broadley et al., 2016) and most importantly (ii) the measured isotopic ratios ^{124}Xe/^{130}Xe and ^{126}Xe/^{130}Xe do not fit the expected cosmogenic production ratios (Fig. S1; Kaiser, 1977).

5.1.3. Z10/6 Barite: 800 °C

Barites heated at 800 °C present a Xe isotopic composition indistinguishable (within 1σ uncertainty) from the modern atmospheric composition with the exception of sample Z10/6 (Fig. 2b). This is in contrast with extractions at higher temperature where all five barites present anomalies up to 100–1000‰ in the light isotopes, fissiogenic isotopes or both, relative to the modern Xe atmospheric composition (Fig. 2c,d and Fig. 3). This strongly suggests that (i) the 800 °C extraction step does not significantly release Xe held in the crystal matrix (which would diffuse out at higher temperature), and (ii) the gas released from Z10/6 at 800 °C was extracted from fluid inclusions that were not released during crushing. Heating at 800 °C thus may have permitted the release of Xe trapped in fluid inclusions by thermal cracking (or decrepitation, Ulrich and Bodnar, 1988). This is supported

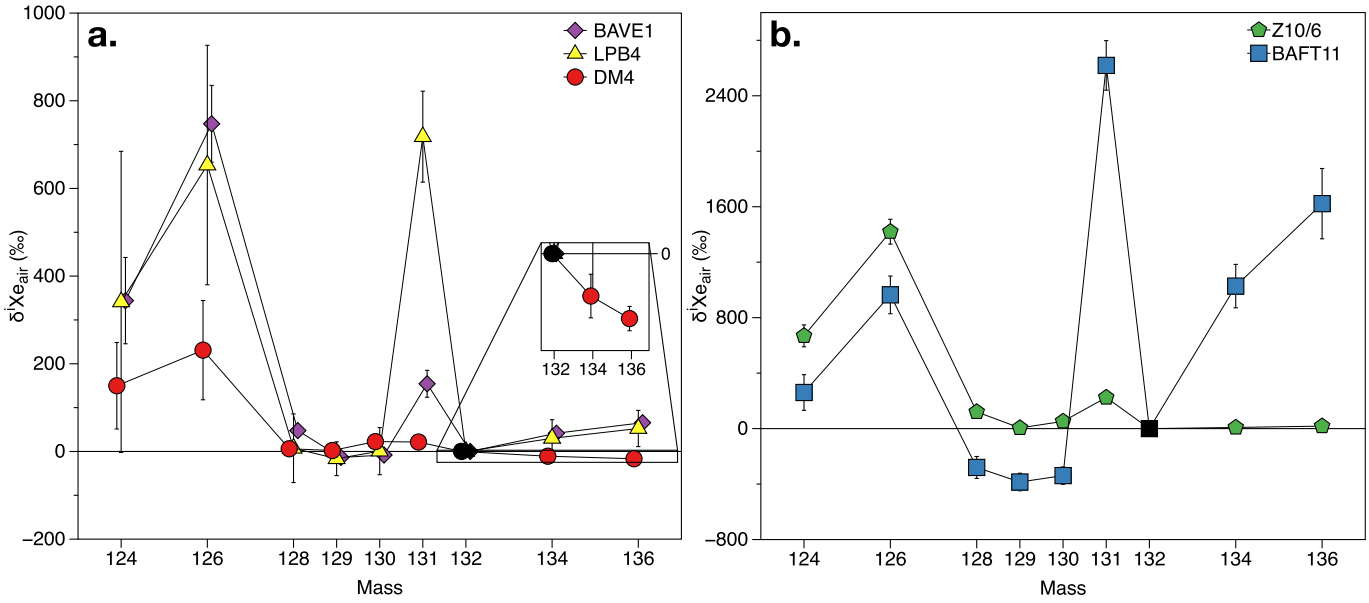

Fig. 3. Isotopic spectrum of Xe released at 1300 °C temperature step of the five sample. a. DM4 in red circles, LPB4 in yellow triangles, BAVE1 in purple diamonds. b. BAFT11 in blue squares, Z10/6 in green pentagrams. Isotopic composition is given using the δ^{i}Xe normalised to ^{132}Xe and the composition of modern atmosphere. Note the change in scale in several hundreds of ‰ compared to extraction 800 °C and crushing (Figs. 1 and 2). Three main signatures are identified here (i) ^{124,126,128}Xe excess coming from spallation production (ii) ^{131}Xe mono-isotopic excess from neutron capture on ^{130}Ba (iii) ^{134,136}Xe from the fission of ^{238}U; ^{132}Xe being also produced by this fission and used for normalization, BAFT11 sample displays virtual depletions of ^{128,129,130}Xe relative to air. The lines joining the symbols are for visual aid. (For interpretation of the references to colour in this figure legend, the reader is referred to the web version of this article.)

by the similarity of the light isotope excesses between crushing and 800 °C extraction step of Z10/6. Although the uncertainties of the crushing extraction are large, such that it is difficult to draw broad conclusions, the agreement between the crushing and 800 °C extractions suggests that both released an ancient atmospheric component. Furthermore, both the crushing and the 800 °C temperature step release a significant amount of fissiogenic Xe, which is not seen in the higher temperature steps. This further confirms the genetic link between the crushing and 800 °C step in the case of Z10/6.

The $^{124\text{-}130}$Xe isotopes gives the degree of MDF for sample Z10/6 to be 11 ± 2.1‰.u^{-1} (1σ, Fig. 2b). Enrichments in the light isotopes of xenon could represent MDF but are also subject to contribution by cosmogenic isotopes. However, in this case we consider the addition of cosmogenic Xe from the matrix to be unlikely for the following reasons. Firstly, as is it the case for sample DM4 (crushing results), the relative ratios of light isotopes do not fit the expected ratios of cosmogenic reactions (Fig. S2), and isotopes produced in the barite matrix are usually released at temperatures higher than 800 °C (Meshik et al., 2001). Secondly, $^{131\text{–}136}$Xe (Xe_f) produced by spontaneous ^{238}U fission are released during crushing and 800 °C heating, but not during higher temperature steps. The extremely low U content of the Z10/6 matrix (below detection <0.07 ppm, Table S1) is consistent with the lack of Xe_f at high temperature. The release of Xe_f at 800 °C however suggests a contribution from the fluid inclusions. Thirdly, if the excesses of light isotopes resulted from a matrix contribution by diffusion, then one should also expect a mono-isotopic excess of ^{131}Xe, as observed at the 1300 °C and 1800 °C extraction steps (Fig. 2c,d), which is not the case at 800 °C or by crushing (Fig. 2a,b). Finally, we observe a similarity in the ^{136}Xe excess of the Xe_f component between crushing (δ^{136}Xe = 105 ± 6‰, Fig. 2a) and 800 °C extraction after considering mass dependent fractionation of 11‰.u^{-1} on the Xe spectrum ($\delta^{136}Xe_{corrected}$ = 136 ± 24‰, Fig. 2b). We therefore consider the addition of cosmogenic Xe from the matrix for sample Z10/6 to be unlikely, whilst acknowledging that it cannot categorically be ruled out.

In sample Z10/6 a depletion of ^{129}Xe relative to the MDF trend (δ^{129}Xe a few ‰ below the MDF regression) is observed in the 800 °C extraction step (Fig. 2b). Such ^{129}Xe depletion relative to the MDF trend has been previously observed in Archean quartz (Avice et al., 2017) and Archean organic matter (Bekaert et al., 2018), but not in Proterozoic and Phanerozoic samples (Avice et al., 2017). This ^{129}Xe deficit is regarded as a potential signature of the Archean atmosphere, which contained less mantle-derived ^{129}Xe than recent atmospheric gases (Avice et al., 2017; Marty et al., 2019). The isotopic spectrum of Xe released from Z10/6 at 800 °C shows a depletion in ^{129}Xe after correction for the isotopic mass dependent fractionation with Δ^{129}Xe = −9.8 ± 7.4‰ (Δ^{129}Xe is defined as the distance between the observed value and that expected for isotope fractionation of modern air, 1σ, Fig. 2b). This observation supports the proposition of a non-linear degassing rate of the mantle through time, with a burst of mantle activity at the end of the Archean around 2.5 Ga, required to explain modern atmospheric ^{129}Xe concentration (Marty et al., 2019).

Samples BAFT11 and BAVE1, although older (3.3 and 3.5 Ga, respectively), do not present any mass-fractionated Xe extracted by crushing or pyrolysis at 800 °C. This infers that (i) the fluid inclusion content in these barites was too low to provide enough Xe concentration for proper analysis and/or (ii) air contamination was too important resulting in the barites to have a modern atmospheric Xe composition, overprinting the Archean component. Future studies utilising barites as a record of the ancient atmosphere should therefore concentrate on obtaining samples with large number of fluid inclusions, where secondary cosmogenic production should be minimal.

5.2. *Secondary contributions from fissiogenic, cosmogenic and radiogenic reactions*

5.2.1. *Identifying the ^{130}Xe excesses*

In order to investigate the radioactive decay of ^{130}Ba to ^{130}Xe, barite samples were heated at sufficient temperature (1300 °C and 1800 °C) to release Xe trapped in the matrix. The half-life of ^{130}Ba has been estimated to be between 6.0 ± 1.1 × 10^{20} yr (Pujol et al., 2009) and 2.2 ± 0.5 × 10^{-21} yr (Meshik et al., 2001), depending on interpretation of cosmogenic contamination on ^{130}Xe (Meshik and Pravdivtseva, 2017). The current recommended value for this half-life is 2.1 (+3.0/−0.8) x 10^{21} yr (Barabash, 2020).

At 1300 °C extraction, cosmogenic (spallation reaction from neutrons on Ba producing $^{124\text{-}131}$Xe, Xe_c) and fissiogenic (spontaneous fission of ^{238}U producing $^{131–136}$Xe, Xe_f) reactions contribute to the ^{130}Xe/^{132}Xe ratio, in addition to radiogenic ^{130}Xe* from ^{130}Ba decay (see 1300 °C release pattern Fig. 3). Therefore, to identify and quantify ^{130}Xe* we need to first correct our spectra from Xe_f and Xe_c production (Fig. S3). The procedure for correcting the Xe isotopic spectra for Xe_f and Xe_c contributions is described in Supplementary Material. After both Xe_f and Xe_c corrections, Z10/6, DM4, LPB4 and BAFT11 barites show small excesses in ^{130}Xe, which likely originates from the decay of ^{130}Ba (see Fig. S3 for BAFT11), and various excesses in ^{131}Xe, up to 3000‰ for barite BAFT11 (see section 5.2.2 ^{131}Xe anomaly).

Sample Z10/6 presents the highest ^{130}Xe* of $1.1 \pm 0.2 \times 10^{-18}$ mol. g^{-1} (where ^{130}Xe* is the difference between ^{130}Xe measured, corrected for Xe_f and Xe_c, and atmospheric ^{130}Xe). Using Meshik et al. (2001)'s or Pujol et al. (2009)'s half-life constants for the radioactive decay of ^{130}Ba gives ages for Z10/6 barite of ~1.5 Ga or 0.4 Ga, respectively. The other barites DM4, LPB4 and BAFT11 show even lower ^{130}Xe* abundances with higher relative uncertainties. Age computation for these barites leads to less that 1 Ga, regardless of the half-life chosen. Given the expected Archean age of these four barites (except for LPB4 dated around 1.8 Ga) and the low ^{130}Xe* (compared to what was obtained for Archean barite by Pujol et al. (2009)), we conclude that these calculated ages do not represent the ages of the barites. This could be the result of the resetting of the ^{130}Ba—^{130}Xe chronometer by some secondary metamorphic process, or as we speculate, it is likely due to the low precision on the ^{130}Xe* calculation presented here. A major source of uncertainty on calculating ^{130}Xe* is the important secondary production of cosmogenic $^{124\text{-}131}$Xe (up to several hundreds for δ^{126}Xe) and the difficulty in precisely quantifying and correcting for it (Meshik and Pravdivtseva, 2017). ^{130}Ba—^{130}Xe dating cannot therefore be readily applied to ancient barites such as those studied here, despite the fact that samples were specifically chosen because of their presumed low exposure to cosmic rays (DM4 and Z10/6 were sampled from within a mine). In fact all samples were exposed to cosmic rays for between 17 Kyr (DM4) and 208 Kyr (Z10/6), which is similar to, but lower, than that previously found in Archean barite (270 Kyr; Srinivasan, 1976). However, the possibility still remains that younger or better shielded samples, with less secondary cosmogenic production, could be used in the future to date barites using the decay of ^{130}Ba, as was previously done in Meshik et al. (2001).

5.2.2. ^{131}Xe anomaly

After correction for Xe_f and Xe_c productions, the high temperature releases present excesses of ^{131}Xe for the five samples (up to 3000‰ for barite BAFT11 from Barberton, South Africa, Fig. S3). Monoisotopic ^{131}Xe production is likely the result of neutron capture reactions on ^{130}Ba (Srinivasan, 1976), with neutrons being mainly produced from uranium and thorium within the barites. ^{238}U produces neutrons directly by spontaneous fission of U and indirectly through α,n reactions on ^{18}O, with the α particles being produced by the radioactive decay of ^{238}U and ^{232}Th. The barite samples include in this study indeed present a correlation ($R^2 = 0.97$) between their U content and their ^{131}Xe/^{132}Xe ratio (Fig. 4). Interestingly, sample Z10/6 has a relatively high δ^{131}Xe of up to 230‰ despite its low U and Th contents (<0.01 ppm). Similar ^{131}Xe excesses have been found in U-free samples by Li et al. (1994) who proposed that they originated from activation by epithermal neutrons from U—Th decay in the surrounding rocks. Epithermal neutrons produced in the surrounding rock units could then interact with nearby barites given that the mean free path is on the order of 1 m in igneous rocks (Li et al., 1994). Z10/6 barite formed as a vein in granitoids, therefore making it more prone to this type of ^{131}Xe production. Our results therefore support the previous observations by Li et al. (1994) that ^{131}Xe excess is essentially a consequence of the presence of U—Th in barites, or, in rare cases, of U—Th within surrounding units.

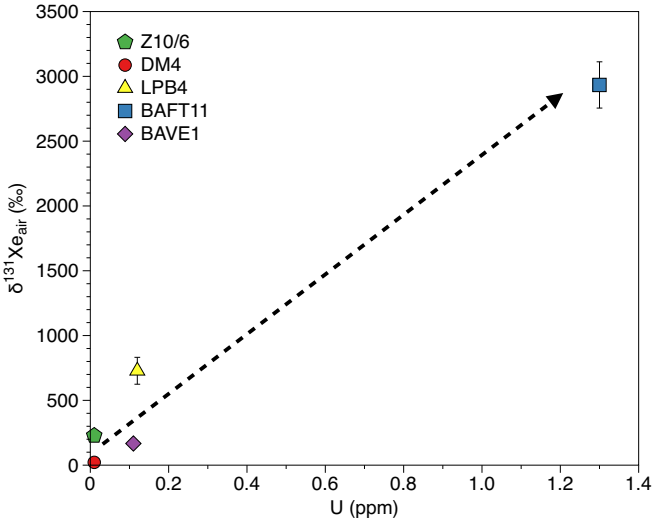

Fig. 4. Correlation between measured δ^{131}Xe versus the U content (ppm) of the five barites analysed for this study. DM4 in red circle, LPB4 in yellow triangle, BAVE1 in purple diamond, BAFT11 in blue square, Z10/6 in green pentagram. Arrow represents the correlation between the U content and the resulting excess of ^{131}Xe from successive nuclear reactions (Section 5.2.2). Arrow fit the data with $R^2 = 0.97$. (For interpretation of the references to colour in this figure legend, the reader is referred to the web version of this article.)

5.3. Evidence for a step evolution of atmospheric Xe isotopes

5.3.1. Observations

The degree of mass dependent Xe fractionation found in Archean-aged samples appears to be correlated with age, with older samples being more fractionated relative to the modern atmospheric composition than younger samples (Pujol et al., 2011; Avice et al., 2018). In the case of a continuous evolution, the degree of MDF of trapped Xe can in principle be used to estimate an approximate MDF Xe age of the barites using the relation between age and MDF (Holland et al., 2013; Bekaert et al., 2018). Bekaert et al. (2018) proposed a power law fit to the evolution of atmospheric MDF-Xe with time, with MDF_{Xe} (‰.u^{-1}) = $0.238*t(Ga)^{3.41}$.

The degrees of MDF-Xe of Z10/6 and DM4 as a function of their estimated ages are shown Fig. 5. The MDF-Xe of Z10/6 does not fit the expected power law when using the proposed barite age of 2.8 Ga (Reimer, 1980). According to the Xe evolution model given above, Z10/6 barite would be 3.1 ± 0.2 Ga (1σ). This hypothesis is improbable because the age of the greenstone formations are unlikely older than 2.9 Ga (Wilson et al., 1995). A similar mismatch between the modelled (by MDF_{Xe} dating) and measured ages has already been identified by Avice et al. (2018) in a 2.74 Ga quartz from Fortescue Group, having a MDF-Xe of 13 ± 1.2‰ u^{-1} (1σ). These two samples (Z10/6 and Fortescue) have MDF-Xe comparable to those of older samples such as Barberton quartz (12.9 ± 1.2‰ u^{-1} at 3.3 ± 0.05 Ga, Avice et al., 2017) or North Pole quartz (15 ± 5‰ u^{-1} at 3.1 ± 0.4 Ga, Pujol et al., 2013). Therefore our data taken together with those from Avice et al. (2018) suggest that the evolution of MDF-Xe was potentially not as regular as previously suggested. These samples instead provide supporting evidence for a plateau in the isotopic evolution of atmospheric Xe between 3.3 Ga and 2.7 Ga, as suggested Fig. 5.

Interestingly, DM4 barite appears to present an unexpectedly low MDF-Xe degree of 3.4 ± 0.5‰.u^{-1}. Using the power law from Bekaert et al. (2018), DM4 barite would have a MDF-Xe age of 2.2 ± 0.1 Gyr which is significantly younger than the Neoarchaean age of the surrounding rocks (Wilson et al., 1995). It is possible that DM4 barite (or its trapped fluid inclusions) could be younger that the host rock formation. However, we also note the striking similarity of DM4 MDF-Xe with that

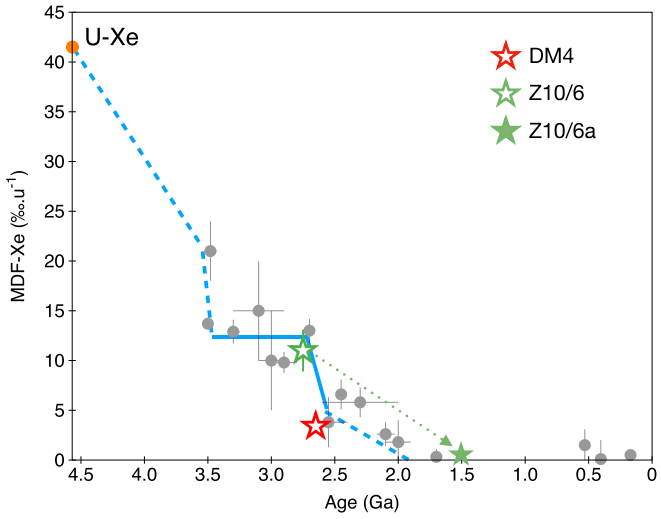

Fig. 5. Evolution of the mass dependent fractionation in ‰.u^{-1} of xenon trapped in samples with variable ages (grey circles, Avice et al. (2018) and ref. therein). U—Xe stands for the initial Xe isotopic composition of the atmosphere (Pepin, 1991). New data from DM4 and Z10/6 samples (from crushing and heating at 800 °C, respectively) are reported as red and green open stars, respectively. Error bars on the age are smaller than symbol size. The green full star represent the potential position of Z10/6a sample if the light isotope excesses are considered spallogenic and not mass-fractionated, and considering the age computed by the ^{130}Ba—^{130}Xe dating system. (For interpretation of the references to colour in this figure legend, the reader is referred to the web version of this article.)

of a 2.55 Ga quartz from Quetico Belt (3.8 ± 2.5‰.u^{-1}, Avice et al., 2018). Taken together, Z10/6 and DM4 MDF support the scenario of a rapid decrease in the atmospheric MDF around 2.5–2.6 Ga (Fig. 5), hence suggesting a disrupted, rather than a regular, evolution of the atmospheric Xe isotopic fractionation over geological periods of time.

Finally, we do not exclude the possibility for the mass fractionation in barite Z10/6 to be the result of secondary cosmogenic production of light Xe isotopes by spallation reaction. If this were the case, sample Z10/6 would not contain any signature of mass fractionated Archean atmosphere. Consequently, to explain why no fractionated ancient atmosphere were found in this fluid inclusion-rich sample, we could consider that the age of the barite was over-estimated. Fig. 5 shows the position Z10/6 would have if it is considered to not contain ancient atmospheric Xe in its fluid inclusion, and assuming that the formation age computed by the ^{130}Ba—^{130}Xe dating system of ~1.5 Ga were accurate.

5.3.2. *Potential implications*

5.3.2.1. Origin of the mass dependent fractionation of atmospheric Xe. The currently favoured explanation to account for both the depletion of atmospheric Xe relative to other noble gases and the evolution of its isotopic composition through time (i.e., the "xenon paradox", Ozima and Podosek (2002)) is the progressive escape to space of Xe^+ ions, dragged away from the Earth by escaping H^+ during the Archean and Hadean eons (Avice et al., 2018; Zahnle et al., 2019).

The evolution of atmospheric Xe isotopes through time therefore relates to how much hydrogen escaped from the Earth, and hence the evolution of Earth's oxidation state over time. However, to account for both Xe's fractionation and depletion, Zahnle et al. (2019)'s hydrodynamic escape model predicts that Xe escape must have been limited to small apertures or short episodes. It suggests that Xe escape was restricted to polar windows by a geomagnetic field, or dominated by outburst of high solar activity, or limited to transient episodes of abundant hydrogen, or a combination of these. These outcomes in Zahnle et al. (2019)'s model appear in very good agreement with our suggestion of a discontinuous (rather than a regular and protracted) evolution of atmospheric Xe's isotope fractionation and escape to space. Better constraining the duration and extent of these bursts of atmospheric Xe escape will be critical to determine the exact amount of H that has been lost to space over geological times, and hence constrain both the evolution of the mass of the ocean and the oxidation of the Earth's surface through time. Given that changes in the atmospheric Xe isotopes through the Archean stop after the Great Oxidation Event (analogous to the disappearance of sulfur mass independent fractionation signatures in sedimentary rocks, S-MIFs, between 2.5 and 2.4 Ga; Warke et al., 2020), Xe systematics potentially also tell us about O_2 and CH_4 levels in the Hadean and Archean atmosphere (Catling and Zahnle, 2020). S-MIFs are indeed considered to result from the UV photolysis of SO_2 in the oxygen poor Archean atmosphere (Farquhar and Wing, 2003), implying that Xe and S isotopic evolution may be conjointly linked to the evolution of the solar UV flux in the Archean.

Whether the atmospheric Xe isotopic composition evolved continuously or discontinuously would have far reaching implications regarding its potential use as a dating tool, for instance concerning the dating of Archean organic matter (Bekaert et al., 2018; Bekaert et al., 2020b) or regarding the determining of the residence time of groundwaters based on their Xe isotopic composition (Holland et al., 2013). Crucially, a discontinuous evolution of atmospheric Xe isotopes would also potentially impact models simulating the onset age of effective volatile recycling by subduction from Xe isotope systematics (Péron and Moreira, 2018; Parai and Mukhopadhyay, 2018). For instance, a step in Xe isotopic evolution at 2.7 Ga potentially indicates that the atmosphere reached a Xe isotopic composition close to modern composition earlier than previously considered. Although it is at present not possible to predict how much a discontinuous evolution of atmospheric Xe through time would impact the times of subduction onset proposed by Péron and Moreira (2018) and Parai and Mukhopadhyay (2018) (roughly 2.8 Ga and 2.5 Ga, respectively), we speculate that the potential for the atmosphere to have reached a modern-like Xe isotopic composition earlier than previously considered may ultimately lead to a revision of the onset of subduction toward older values.

5.3.2.2. An increase in the atmospheric Xe MDF at the end of the Archean?. The MDF-Xe relative to present-day atmosphere decreased over time, progressively making the overall atmospheric Xe budget isotopically heavier with time. However, published data suggest a potential increase of MDF-Xe around 2.5 Ga from 4‰.u^{-1} at 2.6 Ga to 6.6‰.u^{-1} at 2.45 Ga (Venetry belt quartz, Avice et al., 2018). Such an increase could have resulted from the contribution of mantle Xe having a chondritic composition to the already fractionated atmospheric Xe. This would require intense mantle degassing occurring at that time, independently proposed to account for the change of the ^{129}Xe deficit in the Archean atmosphere (Marty et al., 2019). However, mass balance predicts that intense mantle degassing at that time would be insufficient by one order of magnitude to supply enough mantle-derive chondritic Xe to change the MDF-Xe degree of the Archean atmosphere (Supplementary Materials). Therefore we suspect that the apparent MDF-Xe inversion around 2.5 Ga is an artefact on the real evolution of atmospheric Xe due to the lack of precision on both MDF-Xe calculation and sample ages. Improving the precision of atmospheric Xe's isotopic evolution through time will help better understand the process(es) and conditions under which it was mass fractionated. Specifically, more constraints on Xe atmospheric fractionation around 2.7–2.4 Ga appear to be critical to better understand the atmospheric hydrodynamic processes that led to the Great Oxidation Event between 2.50 Ga and 2.43 Ga (Sessions et al., 2009; Warke et al., 2020).

6. Conclusion

We analysed the Xe isotopic composition of five barites dated from

3.5 Ga to 1.8 Ga through crushing and step-heating. Extractions at high temperature (1300 °C and 1800 °C) revealed variable excesses in ^{131}Xe isotope for the five barites, up to 3000% for barite BAFT11, resulting from neutron capture on ^{130}Ba. ^{130}Xe excesses were also identified, but too low to compute ages using the ^{130}Ba—^{130}Xe radioactive decay because of important contributions from the secondary production of cosmogenic xenon isotopes ^{124,126,128,129,130}Xe. Crushing and heating at 800 °C revealed for two barites, DM4 and Z10/6 which contained sufficient fluid inclusions, the isotopic composition of Xe in the atmosphere when they formed. DM4 (~2.6 Ga) and Z10/6 (~2.8 Ga) barites present a Xe isotopic signature mass dependently fractionated by 3.4 ± 0.5‰. u^{-1} and 11 ± 2.1‰.u^{-1}, respectively, relative to the modern atmosphere. Along with previous analyses of Xe in Archean rocks, these results potentially show a step at 2.7 Ga in the evolution of the atmospheric MDF-Xe degree. This suggests that the process fractionating xenon isotopes was discontinuous in time, rather than a regular evolution as previously thought. The main consequence of this observation is the reconsideration of the use of the MDF-Xe degree as a dating tool for Archean aged samples or models of volatile recycling initiation.

The following are the supplementary data related to this article.

Data availability

All data produced and used in this study are given in the excel files in the Supplementary Material.

Declaration of Competing Interest

The authors declare that they have no known competing financial interests or personal relationships that could have appeared to influence the work reported in this paper.

Acknowledgments

This work was funded by the ERC grant No. 695618 to B.M. We thank the S.A.R.M for providing elemental bulk analyses of the barites. We thank Laurent Zimmerman for technical mentorship and assistance. We thank David Byrne for fruitful discussions. We thank the three anonymous reviewers for their comments and suggestions, which significantly improved the paper. This is CRPG contribution 2786.

Appendix A. Supplementary data

Supplementary data to this article can be found online at https://doi.org/10.1016/j.chemgeo.2021.120405.

References

Abbott, D.H., Isley, A.E., 2002. The instensity, occurrence, and duration of superplume events and eras over geological time. J. Geodyn. 34, 265–307. https://doi.org/10.1016/S0264-3707(02)00024-8.

Avice, G., Marty, B., Burgess, R., 2017. The origin and degassing history of the Earth's atmosphere revealed by Archean xenon. Nat. Commun. 8, 1–9. https://doi.org/10.1038/ncomms15455.

Avice, G., Marty, B., Burgess, R., Hofmann, A., Philippot, P., Zahnle, K., Zakharov, D., 2018. Evolution of atmospheric xenon and other noble gases inferred from Archean to Paleoproterozoic rocks. Geochim. Cosmochim. Acta 232, 82–100. https://doi.org/10.1016/j.gca.2018.04.018.

Barabash, A., 2020. Precise Half-Life Values for Two-Neutrino Double-β Decay: 2020 Review. Universe 6 (10), 159.

Basford, J.R., Dragon, J.C., Pepin, R.O., Coscio Jr., M.R., Murthy, V.R., 1973. Krypton and xenon in lunar fines. In: Proceedings of the 4th Lunar Science Conference, pp. 1915–1955.

Bekaert, D.V., Broadley, M.W., Delarue, F., Avice, G., Robert, F., Marty, B., 2018. Archean kerogen as a new tracer of atmospheric evolution: Implications for dating the widespread nature of early life. Sci. Adv. 4, 1–23. https://doi.org/10.1126/sciadv.aar2091s.

Bekaert, D.V., Broadley, M.W., Marty, B., 2020a. The origin and fate of volatile elements on Earth revisited in light of noble gas data obtained from comet 67P/Churyumov-Gerasimenko. Sci. Rep. 10, 1–18. https://doi.org/10.1038/s41598-020-62650-3.

Bekaert, D.V., Broadley, M.W., Delarue, F., Druzhinina, Z., Paris, G., Robert, F., Sugitani, K., Marty, B., 2020b. Xenon isotopes in Archean and Proterozoic insoluble organic matter: a robust indicator of syngenecity? Precambrian Res. 336, 105505. https://doi.org/10.1016/j.precamres.2019.105505.

Broadley, M.W., Ballentine, C.J., Chavrit, D., Dallai, L., Burgess, R., 2016. Sedimentary halogens and noble gases within Western Antarctic xenoliths: Implications of extensive volatile recycling to the sub continental lithospheric mantle. Geochim. Cosmochim. Acta 176, 139–156. https://doi.org/10.1016/j.gca.2015.12.013.

Cadogan, P.H., 1977. Palaeoatmospheric argon in Rhynie chert. Nature 268, 38–41. https://doi.org/10.1038/268038a0.

Carignan, J., Hild, P., Mevelle, G., Morel, J., Yeghicheyan, D., 2001. Routine analyses of trace elements in geological samples using flow injection and low pressure on-line liquid chromatography coupled to ICP-MS: a study of geochemical reference materials BR, DR-N, UB-N, AN-G and GH. Geostand. Newslett. 25, 187–198. https://doi.org/10.1111/j.1751-908x.2001.tb00595.x.

Catling, D.C., Zahnle, K.J., 2020. The Archean atmosphere. Sci. Adv. 6, eaax1420.

Claire, M.W., Sheets, J., Cohen, M., Ribas, I., Meadows, V.S., Catling, D.C., 2012. The evolution of solar flux from 0.1 nm to 160 μm: Quantitative estimates for planetary studies. Astrophys. J. 757 https://doi.org/10.1088/0004-637X/757/1/95.

Drabon, N., Galić, A., Mason, P.R., Lowe, D.R., 2019. Provenance and tectonic implications of the 3.28–3.23 Ga Fig tree Group, Central Barberton greenstone belt, South Africa. Precambrian Res. 325, 1–19.

Farquhar, J., Wing, B.A., 2003. Multiple sulfur isotopes and the evolution of the atmosphere. Earth Planet. Sci. Lett. 213, 1–13. https://doi.org/10.1016/S0012-821X(03)00296-6.

Geng, H., Brandl, G., Sun, M., Wong, J., Kröner, A., 2014. Zircon ages defining deposition of the palaeoproterozoic soutpansberg group and further evidence for eoarchaean crust in South Africa. Precambrian Res. 249, 247–262. https://doi.org/10.1016/j.precamres.2014.05.020.

Gumsley, A.P., Chamberlain, K.R., Bleeker, W., Söderlund, U., De Kock, M.O., Larsson, E. R., Bekker, A., 2017. Timing and tempo of the great oxidation event. Proc. Natl. Acad. Sci. U. S. A. 114, 1811–1816. https://doi.org/10.1073/pnas.1608824114.

Hébrard, E., Marty, B., 2014. Coupled noble gas-hydrocarbon evolution of the early Earth atmosphere upon solar UV irradiation. Earth Planet. Sci. Lett. 385, 40–48. https://doi.org/10.1016/j.epsl.2013.10.022.

Heinrichs, T.K., Reimer, T.O., 1977. A sedimentary barite deposit from the Archean Fig tree Group of the Barberton Mountain Land (South Africa). Econ. Geol. 72, 1426–1441. https://doi.org/10.2113/gsecongeo.72.8.1426.

Hirsch, M., Muto, K., Oda, T., Klapdor-Kleingrothaus, H.V., 1994. Nuclear structure calculation of β+β+, β+/EC and EC/EC decay matrix elements. Zeitschrift für Phys. A Hadron. Nucl. 347, 151–160. https://doi.org/10.1007/BF01292371.

Holland, G., Lollar, B.S., Li, L., Lacrampe-Couloume, G., Slater, G.F., Ballentine, C.J., 2013. Deep fracture fluids isolated in the crust since the Precambrian era. Nature 497, 357–360.

Huston, D.L., Logan, G.A., 2004. Barite, BIFs and bugs: Evidence for the evolution of the Earth's early hydrosphere. Earth Planet. Sci. Lett. 220, 41–55. https://doi.org/10.1016/S0012-821X(04)00034-2.

Jelsma, H.A., Dirks, P.H., 2002. Neoarchaean tectonic evolution of the Zimbabwe Craton. Geol. Soc. Spec. Publ. 199 (1), 183–211.

Kaiser, W.A., 1977. The excitation functions of Ba (p, X) ^{M} Xe (M — 124-136) in the energy range 38-600 MeV; the use of 'cosmogenic' xenon for estimating 'burial' depths and 'real' exposure ages. Philos. Trans. R. Soc. London. Ser. A Math. Phys. Sci. 285, 337–362. https://doi.org/10.1098/rsta.1977.0074.

Lee, J.Y., Marti, K., Severinghaus, J.P., Kawamura, K., Yoo, H.S., Lee, J.B., Kim, J.S., 2006. A redetermination of the isotopic abundances of atmospheric Ar. Geochim. Cosmochim. Acta 70, 4507–4512. https://doi.org/10.1016/j.gca.2006.06.1563.

Li, B., Lee, J.T., Manuel, O.K., 1994. Anomalous 131Xe in barites. Earth Planet. Sci. Lett. 123, 71–79. https://doi.org/10.1016/0012-821X(94)90258-5.

Marty, B., Altwegg, K., Balsiger, H., Bar-Nun, A., Bekaert, D.V., Berthelier, J.J., Bieler, A., Briois, C., Calmonte, U., Combi, M., De Keyser, J., Fiethe, B., Fuselier, S.A., Gasc, S., Gombosi, T.I., Hansen, K.C., Hässig, M., Jäckel, A., Kopp, E., Korth, A., Le Roy, L., Mall, U., Mousis, O., Rème, H., Owen, T., Rubin, M., Sémon, T., Tzou, C.Y., Waite, J. H., Wurz, P., 2017. Xenon isotopes in 67P/Churyumov-Gerasimenko show that comets contributed to Earth's atmosphere. Science (80-.) 356, 1069–1072. https://doi.org/10.1126/science.aal3496.

Marty, B., Bekaert, D.V., Broadley, M.W., Jaupart, C., 2019. Geochemical evidence for high volatile fluxes from the mantle at the end of the Archaean. Nature 575, 485–488. https://doi.org/10.1038/s41586-019-1745-7.

Meshik, A., Pravdivtseva, O., 2017. Weak Decay of Tellurium and Barium Isotopes in Geological Samples: Current Status, 020702, pp. 2016–2018. https://doi.org/10.7566/jpscp.14.020702.

Meshik, A.P., Hohenberg, C.M., Pravdivtseva, O.V., Kapusta, Ya.S., 2001. Weak decay of 130Ba and 132Ba: geochemical measurements. Phys. Rev. C 64, 352051–352056. https://doi.org/10.1103/PhysRevC.64.035205.

Ozima, M., Podosek, F.A., 2002. Noble gas Geochemistry, second ed. Cambridge University Press, Cambridge.

Parai, R., Mukhopadhyay, S., 2018. Xenon isotopic constraints on the history of volatile recycling into the mantle. Nature 560, 223–227.

Pepin, R.O., 1991. On the origin and early evolution of terrestrial planet atmospheres and meteoritic volatiles. Icarus 92, 2–79. https://doi.org/10.1016/0019-1035(91)90036-S.

Péron, S., Moreira, M., 2018. Onset of volatile recycling into the mantle determined by xenon anomalies. Geochemical Perspect. Lett. 9, 21–25. https://doi.org/10.7185/geochemlet.1833.

Porcelli, D., Ballentine, C.J., 2002. Models for distribution of terrestrial noble gases and evolution of the atmosphere. Rev. Mineral. Geochem. 47, 411–480.

Pujol, M., Marty, B., Burnard, P., Philippot, P., 2009. Xenon in Archean barite: Weak decay of 130Ba, mass-dependent isotopic fractionation and implication for barite formation. Geochim. Cosmochim. Acta 73, 6834–6846. https://doi.org/10.1016/j.gca.2009.08.002.

Pujol, M., Marty, B., Burgess, R., 2011. Chondritic-like xenon trapped in Archean rocks: a possible signature of the ancient atmosphere. Earth Planet. Sci. Lett. 308, 298–306. https://doi.org/10.1016/j.epsl.2011.05.053.

Pujol, M., Marty, B., Burgess, R., Turner, G., Philippot, P., 2013. Argon isotopic composition of Archaean atmosphere probes early Earth geodynamics. Nature 498, 87–90. https://doi.org/10.1038/nature12152.

Reimer, T.O., 1980. Archean sedimentary baryte deposits of the Swaziland Supergroup (Barberton Mountain Land, South Africa). Precambrian Res. 12, 393–410. https://doi.org/10.1016/0301-9268(80)90037-6.

Reimer, T.O., 1990. Archaean barite deposits of Southern Africa. J. Geol. Soc. India 35, 131–150.

Reimer, T.O., 1995. The Proterozoic baryte deposits of southern Africa. In: Barton, J.M., Copperthwaite, Y.E. (Eds.), Extended Abstracts, Centennial Geocongress. Rand Afrikaans University, Johannesburg, pp. 99–102.

Ribas, I., Guinan, E.F., Gudel, M., Audard, M., 2005. Evolution of the Solar activity over Time and Effects on Planetary Atmospheres. I. High-Energy Irradiances (1–1700 a). Astrophys. J. 622, 680–694. https://doi.org/10.1086/427977.

Sessions, A.L., Doughty, D.M., Welander, P.V., Summons, R.E., Newman, D.K., 2009. The continuing puzzle of the great oxidation event. Curr. Biol. 19, R567–R574.

Srinivasan, B., 1976. Barites: anomalous xenon from spallation and neutron-induced reactions. Earth Planet. Sci. Lett. 31, 129–141. https://doi.org/10.1016/0012-821X(76)90104-7.

Stuart, F.M., Mark, D.F., Gandanger, P., McConville, P., 2016. Earth-atmosphere evolution based on new determination of Devonian atmosphere Ar isotopic composition. Earth Planet. Sci. Lett. 446, 21–26. https://doi.org/10.1016/j.epsl.2016.04.012.

Ulrich, M.R., Bodnar, R.J., 1988. Systematics of stretching of fluid inclusions; II, Barite at 1 atm confining pressure. Econ. Geol. 83, 1037–1046.

Van Kranendonk, M.J., Kröner, A., Hegner, E., Connelly, J., 2009. Age, lithology and structural evolution of the c. 3.53 Ga Theespruit Formation in the Tjakastad area, southwestern Barberton Greenstone Belt, South Africa, with implications for Archaean tectonics. Chem. Geol. 261, 115–139. https://doi.org/10.1016/j.chemgeo.2008.11.006.

Vermeesch, P., 2018. IsoplotR: a free and open toolbox for geochronology. Geosci. Front. 9, 1479–1493. https://doi.org/10.1016/j.gsf.2018.04.001.

Warke, M.R., Di Rocco, T., Zerkle, A.L., Lepland, A., Prave, A.R., Martin, A.P., Ueno, Y., Condon, D.J., Claire, M.W., 2020. The great oxidation event preceded a paleoproterozoic "snowball earth". Proc. Natl. Acad. Sci. U. S. A. 117, 13314–13320. https://doi.org/10.1073/pnas.2003090117.

Wilson, J.F., Nesbitt, R.W., Fanning, C.M., 1995. Zircon geochronology of Archaean felsic sequences in the Zimbabwe craton: a revision of greenstone stratigraphy and a model for crustal growth. Geol. Soc. Spec. Publ. 95, 109–126. https://doi.org/10.1144/GSL.SP.1995.095.01.07.

Yokochi, R., Marty, B., Pik, R., Burnard, P., 2005. High ^{3}He/^{4}He ratios in peridotite xenoliths from SW Japan revisited: Evidence for cosmogenic ^{3}He released by vacuum crushing. Geochem. Geophys. Geosyst. 6, n/a. https://doi.org/10.1029/2004GC000836.

Zahnle, K.J., Gacesa, M., Catling, D.C., 2019. Strange messenger: a new history of hydrogen on Earth, as told by Xenon. Geochim. Cosmochim. Acta 244, 56–85. https://doi.org/10.1016/j.gca.2018.09.017.

Zimmermann, L., Avice, G., Blard, P.H., Marty, B., Füri, E., Burnard, P.G., 2018. A new all-metal induction furnace for noble gas extraction. Chem. Geol. 480, 86–92. https://doi.org/10.1016/j.chemgeo.2017.09.018.